Modeling the affect of multiple beam clipping in FIR and sub-millimetre instrumentation: ISO-LWS and FIRST-SPIRE

Authors: Martin Caldwell, Bruce Swinyard, Peter Gray. Space Science Department, Rutherford Appleton Laboratory, CLRC, Chilton, Didcot, OX11 OQX, UK. Tel.(44) 1235 4586 Fax.(44) 1235 446667 E-mail m.caldwell@rl.ac.uk.

Keywords: Diffraction, long wavelength, sub-millimetre, field-of-view response, stray-light.

ABSTRACT.

At short wavelengths optical systems can be designed such that a single aperture defines the beam that is used (system light gathering power), and another (the system field stop) defines the field-of-view (FOV). These components define the beam envelope and all other components are oversized so that they do not 'clip' or vignette this envelope.

At longer wavelengths the diffraction caused by such clipping can seriously degrade the FOV response function and cause an increase in stray-light background. It is thus even more desirable to avoid clipping the beam as it passes through an instrument by oversizing all the optical elements. In space borne instruments, however, accommodation constraints can turn such oversizing into an unaffordable luxury. Instrument design must therefore consider the impact of multiple beam clipping and in particular any degradation in the FOV function.

In this paper we describe such an analysis, based on advanced ray-tracing software, and give results for its application to two instruments:

1. The infra-red space observatory Long Wavelength Spectrometer (ISO-LWS, wavelength range 46-198 μm), where the FOV response is modeled for use with on-board calibration and data retrieval.

2. The imaging photometer in the Far Infra-Red Space Telescope SPIRE instrument (Spectral & Photometric Imaging Receiver, wavelength range 200-650 μm), where the analysis is needed for (a) Trade-off studies between instrument sensitivity (aperture size) and FOV degradation by clipping (b) Predicting the FOV performance of the final proposed design.

CONTENTS.

1. Beam clipping in short-wavelength optics.

2. Longer wavelength systems.

3. Case with multiple beam-clipping (MBC).

4. Beam propagation method & Numerical restrictions.

    4.1 Far-field case.

    4.2 Near-field case.

5. Long-wave-spectrometer (LWS) instrument on infra-red space observatory (ISO).

6. Spectral & photometric imaging receiver (SPIRE) instrument on far-infra-red space telescope (FIRST).

7. Conclusion.

8. Acknowledgements.

9. References.

1. BEAM CLIPPING IN SHORT-WAVELENGTH OPTICS.

Figure 1 shows a schematic of the beam clipping which occurs in a conventional optical system. For simplicity a system consisting of 1 optic is shown, with the minimum 2 stops present; a system aperture stop to define the beam collection aperture (F-number), and a system field stop to define the field-of-view (FOV). These stops define the geometric beam envelope, i.e. the A-Ω of the system. If we wish that the response is set by beam clipping at only these stops, all of the other components, e.g. the lens shown, are oversized with respect to this beam envelope.

Assuming for now that the detector is a fully incoherent type, the FOV response is the relative amount of energy arriving at the detector as the source incident angle β is varied. This energy is given by the integral of the image plane intensity distribution (the system point source transmittance function PST [1]) over the detector active area (given by the normalised detector spatial response function R) . This gives

$$FOV(\beta) = \int PST(\beta', \beta) R(\beta').d\beta' \quad (1a)$$

where β‘ is the lateral position co-ordinate at the detector plane (in two-dimensions), expressed in terms of equivalent angle in object space (in this angular co-ordinate system R may be termed the ‘geometric footprint’ of the system on the object).

If the PST shows negligible variation with beam angle β, over the range of interest, we may use just the PST response of the on-axis beam, i.e. PST(β‘,β=0). Writing this as a function of one variable:

$$PST_O(\beta') = \mathrm{PST}(\beta', 0) \quad (1b)$$

The FOV equation becomes a simple convolution:

$$FOV(\beta) = \int PST_O(\beta' - \beta) R(\beta').d\beta' \quad (1c)$$

The range required is usually that up to the point where the FOV drops to a level below the noise floor of the instrument. This form for FOV is then valid providing that, over this β-range:

1. The aberrations don’t change significantly.
2. The components can be oversized adequately to ensure that they add no extra clipping.

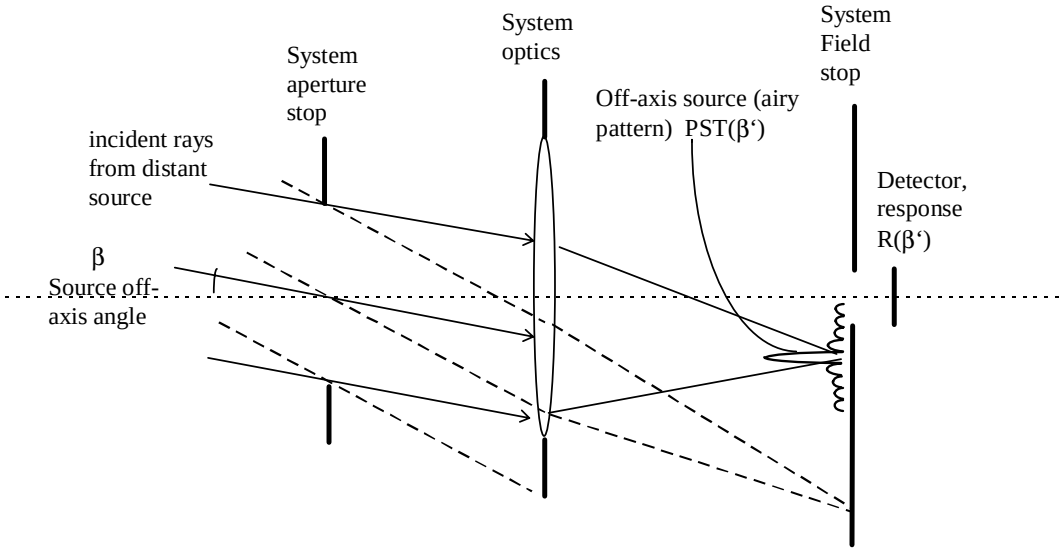

Fig. 1a. Beam clipping, short-wavelength case.

2. LONGER WAVELENGTH SYSTEMS.

Figure 1b. shows the picture of fig.1a modified for the case of a longer wavelength system. Here we assume the only dimension which is changed is that of the wavelength (this occurs in practice in a space instrument when accommodation constraints prevent the instrument apertures and focal length being scaled with wavelength). The main difference to fig.1a is the increased width of the beam in both the near-field (e.g. increased size at the lens with respect to the geometric beam) and in the far-field (width of the PSF). The central maximum has a radius which in angular terms in object space (as shown in the figure) is given by $\beta_o \approx \lambda/D$.

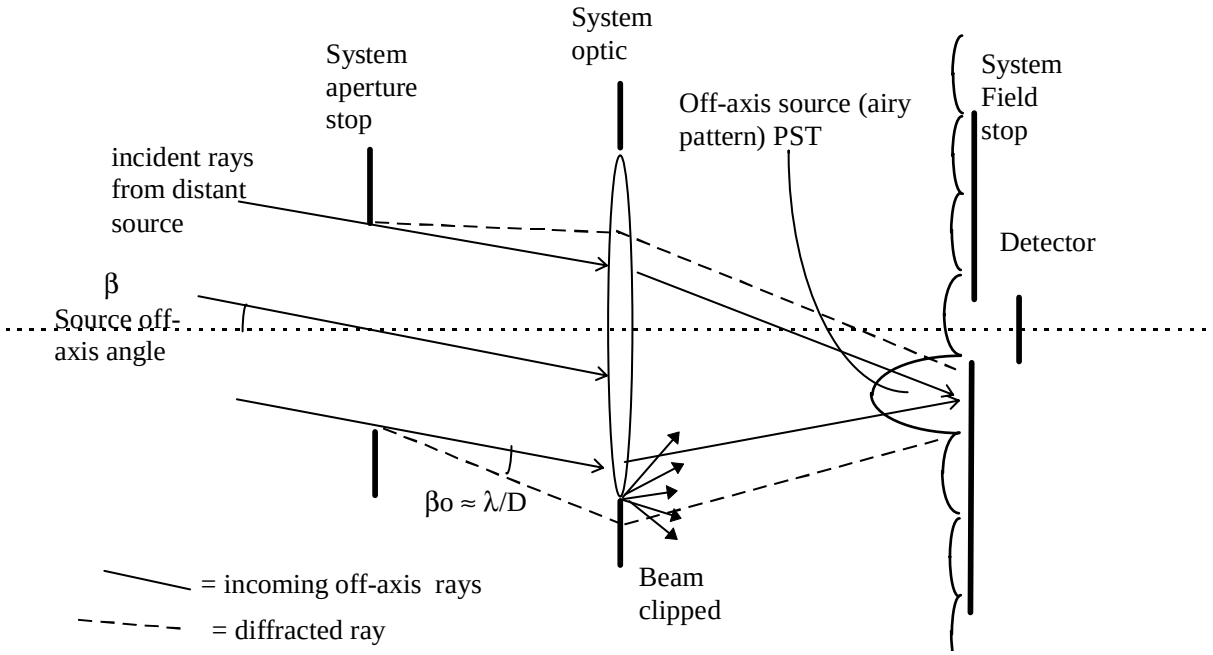

Fig.1b. Beam clipping, long wavelength case.

The figure illustrates the difficulty of maintaining the 'oversize' criteria at longer wavelengths. Two effects can be noted:

1. The used beam as defined by the system aperture stop has significant diffractive spreading, so that at components remote from a pupil plane (e.g. the lens in fig.1b) it is now significantly wider than the geometric beam envelope. The effect could lead to clipping even at a small off-axis angle β. For example, the instruments described here have D~50mm, λ~0.2mm and component separations L~200mm. The fractional increase in beam width due to diffraction is then ~ $2.\lambda L/D^2$ = 3 %.

2. The PST function is now wider, with its 'wings' extending farther across the image plane. This means that the FOV response may remain at a significant level (compared to the system noise), to much larger values of β than in the short-λ case.

These effects are indicative of the increasing importance of coherence properties at longer wavelengths, and as a result such systems may be designed using quasi-optics methods [2]. This involves to a description of the overall beam shape as the superposition of a set of beam-modes, which can then be propagated separately using the ABCD formalism. It is most suitable for coherent systems (characterised by $A\Omega \approx \lambda^2$) where the pattern can be described using relatively few modes. Since a coherent detector behaves as a point source, in this case the response function FOV(β) is given by the PST alone, and the convolution of equation (1c) is not required.

The systems considered here have low coherence, and the number of modes needed to describe the beam at a single source angle β is consequently relatively very large. In these circumstances a ray-trace based model for beam propagation (described later) is a more efficient method of analysis than the beam-mode method.

It can be seen from figure 1b that a system designed using ray-tracing (or quasi-optics) may produce significant beam clipping at components other than those which are intended to define the beam. In such cases the above assumptions and equations for FOV (which are only valid up to angles where beam clipping becomes significant) no longer apply. Such is the case in the instruments of interest here.

3. CASE WITH MULTIPLE BEAM-CLIPPING (MBC).

In the instruments considered here beam clipping becomes important in the design because the optics accommodation constraints make it impossible to provide the component oversizes required at long wavelengths, without a serious loss of collection aperture, at all wavelengths. The instrument design, especially in cases with large wavelength coverage, then involves a trade-off between the loss of throughput and the long-wavelength stray light problems introduced by MBC.

Other relevant features of these instruments are:

- At long wavelengths the on-board stray light is dominated by edge-diffraction rather than the incoherent surface scatter (e.g. from micro-roughness or particle contamination) which dominates at shorter wavelengths.

- The typical strategy to defend against on-board thermal emission is to have the optics enclosed in boxes of progressively lower temperature at each stage of imaging, with stray light blocking implemented by apertures & filters, and the detector in the smallest, coldest box.

The MBC gives two main degradations to instrument performance:

1. The FOV response will be broadened, possibly with added side-lobes due to the added diffraction from optical components.

2. Where the beam is 'clipped' the portion not transmitted by the component will be incident on or subsequently reflected to some internal baffle surface. Where this is in the relatively hot outer structure it can contribute significant unwanted background radiance to the detector.

In the cases of figs. 1 & 2 above, if either the range of β considered is extended, or if component oversize is reduced, we eventually find clipping at other apertures, for example in the incident beam shown by the dashed lines in fig.1a, significant clipping is occurring at the optical element. At this point the beam aperture begins to be reduced and so the PST (or antenna pattern) widens. The assumption that it is independent of β is then no longer valid, and we must return to the general form of FOV in equation 1. The computation then requires a propagation analysis repeated over all relevant incident angles, leading to a much larger calculation than in the cases without MBC, where a single propagation analysis was used. There may be computational efficiency advantages to be gained by propagating the beam in the forward or reverse direction, and in the instruments analysed here both types of model are used. Usually the propagation is first analysed for just the on-axis & the maximum β-range cases, in order to assess how much the PST is being changed by the MBC effect

4. BEAM PROPAGATION METHOD & NUMERICAL RESTRICTIONS.

The method used is that of 'decomposition' of the beam pattern into a set of rays [3], which can then be ray-traced within a conventional optical design program [4] to a subsequent plane where the beam pattern is reconstructed from the ray set. In order to describe diffraction effects in a complex-amplitude optical field, the ray set must include extra rays in addition to those used to describe incoherent geometric effects in standard ray-trace packages. The resulting ray set is related to the 'Gabor representation' of a coherent field [5] .

For our purposes the beam must be 'decomposed' at each component at which clipping occurs, and the decomposition algorithms currently available are of 2 types:

1. For far-field regions, where the beam diameter is many wavelengths. Here the ray set used is a spatial array of rays, with directions each parallel to the local Poynting vector of the beam (fig.3).

2. For near-field regions, where the beam diameter is a few wavelengths or less (focused beam). Here the ray set is an angular array of rays generated at a single point at the beam centre (a 'cone' of rays emanating from the focal point).

The method has certain sampling limitations similar to those arising in Fourier Analysis [6]. Consider a beam pattern calculated over an analysis window (perpendicular to the beam) of half-aperture W, in N x N pixels. The spatial resolution to which the diffracting edge is defined is then $\Delta x = 2W/N$. For a physically representative analysis of a sharp diffracting edge we should increase N to decrease Δx. However, the diffraction angle range required to describe the pattern to resolution Δx is $\Delta\theta \approx \lambda/\Delta x$, so as we approach $\Delta x < \lambda$ the angular range of the ray-set required becomes large [7]. Moreover the synthesis of such a set often requires a more general model than those currently available (this case is intermediate between the far- & near-field analyses cases, & the required ray-set is closer to the Gabor representation[5]). In addition a very large analysis window is needed at the next optic, to collect the rays. Lastly, the diffraction theory on which the method is based gives only a limited description of electromagnetic effects on this scale [8]. For these reasons the analyses to date are limited and cannot describe clipping to arbitrarily fine resolution $\Delta x << \lambda$.

Added to this is the issue of computation time, which can be excessive given that the typical ray-set required has NxN rays, each contributing to NxN pixels in the pattern at the next optic (so the calculation time scales as N^4). This problem of modeling larger diffraction angles (higher spatial resolution) arises similarly in Fourier Optics and in numerical diffraction integral methods used in mm-waves [6,9].

In our instruments beam clipping is more common at components of the far-field type; components near foci regions are normally easily oversized with respect to the detector (system field stop) to avoid clipping , whereas for the larger far-field components sufficient oversize is much more difficult to accommodate.

4.1. FAR-FIELD CASE.

Here the clipping is described as shown in fig.3. To correctly describe the clipping the incoming beam (in this case a full gaussian) is decomposed at the plane containing the component's edge (the clipping component is usually either a planar stop or a curved mirror). Of the new set of rays, those lying outside of the component edge then fail to be traced onwards, and the remainder describe the clipped beam (part-truncated gaussian).

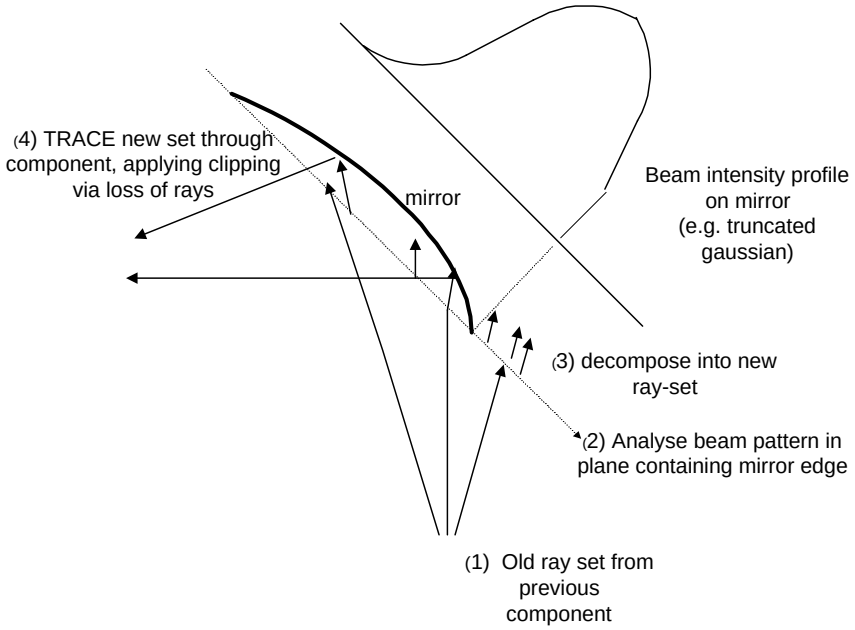

Fig.3. Process of beam decomposition used to describe far-field beam clipping.

For beam analysis in far-field regions there are currently two numerical limitations.

Firstly, the limitations noted above put a restriction on the 'sharpness' of the edge that can be analysed at any particular wavelength; the best spatial resolution available is $\Delta x \approx \lambda$. For example at the longest wavelength of 0.5mm considered here, the analysis is limited to that for a 'soft' edge whose transmission profile is blurred over approximately this dimension. The corresponding maximum allowed pixel number is given by $N_{max} \approx 2W/\lambda$.

Secondly, there is a requirement that the pixel size is small enough that the phase change of the wavefront across the aperture can be described without numerical aliasing. This requires that the pixel spacing is always less than the width of the Fresnel zone in which it lies. For a spherical wavefront with ROC = R, the limiting case occurs at the edge of the aperture (the narrowest zone) and it leads to a minimum pixel number needed of

$N_{min} > W/(2F\lambda)$.

For many reflective components the clipping edge is tilted with respect to the incident beam, since the components are off-axis conic-section mirrors used at e.g. 10 to 30 degrees angle of incidence. In these cases the tilted window leads to modification of the above equations.

In our instruments, where typically W=2cm and minimum f-number of the beam is F=R/2W = 3, the above equations give

$72 < N < 869$ for the shortest wavelength used (46μm)

$7 < N < 87$ for the longest wavelength (0.5mm)

The maximum allowed N is the one used for accurate computations, while lower N is used for initial analyses.

4.2 NEAR-FIELD CASE.

For beam-clipping in the near field, the decomposition is performed in terms of the angular spectrum of the beam. Here the clipping has to be applied to the optical field before the new ray-set is generated. In this case edges can be described to finer detail of $\Delta x < \lambda$, but the above diffraction considerations still impose a limit , due to the finite angular range allowable for the new ray-set (i.e. less than a hemisphere[7]). In our models, Δx is automatically chosen such that the ray-set angular range is some 'oversize' factor (of typically x2 to x4) times the geometric beam divergence. This is usually sufficient to describe the 'wings' of the beam pattern down to sufficient levels of energy.

5. LONG-WAVE-SPECTROMETER (LWS) INSTRUMENT ON INFRA-RED SPACE OBSERVATORY (ISO).

The LWS instrument is a grating spectrometer currently operating on board ESA's ISO mission, and it is shown in fig.4. LWS is of particular interest here because the PST measured in flight has a FWHM of 90 arcminutes, approx. 13% narrower than that predicted [10],implying that some unexpected beam-clipping is occurring. Moreover the spectral response , when plotted versus wavenumber, shows an unexpected periodic variation, implying that some multiple-reflection Fabry-Perot effect is occurring. The frequency period of this corresponded to a free-space path length difference of 1.3mm, and this dimension was then traced to the height of the field mirror (M2 near the top centre in figure 4) above its mounting surface. The conclusions were that:

1. This focal-plane mirror was clipping the beam (whereas the design was for the field-stop formed by the edge of the mirror to be oversized with respect to that formed by the detector).

2. For the part of the beam lying outside the edge of the mirror, the reflectivity of the surround was none-zero, allowing this part of the beam to reflect back along the optical path & so re-join the main beam, to produce the Fabry-Perot fringing seen in the spectral response.

The conclusion 1. is also consistent with the feature that the measured PSF is narrower than that expected.

Here we look at the consequences of 1. for the instrument PSF, by making a multiple-beam-clipping analysis on the system geometry. The ray-trace model is shown in fig.4b, in the same orientation as fig.4a, with the ISO telescope included. The degree of by which the PST is narrowed was found to vary with wavelength, and it is significant even at the shortest wavelength (46μm), i.e. that at which MBC should be least significant. This is the wavelength modeled here.

The field mirror M2 is at a focal plane. In this instrument detectors with low spatial coherence are used, and so the beam pattern is that from a point source incident from infinity at angle β, clipped by the system pupil (located at the telescope secondary). The propagation analysis proceeds in the forward direction, and figure 5 shows a cross-section of the beam pattern at the telescope primary mirror. Here the intensity distribution is approximately a 'top-hat', with a central obscuration due to the secondary, but the effect of the telescope spider is not included. The pattern at M2 is shown in fig. 6a, in contour plot, and as this is a focal plane the beam shape is close to that of the Airy pattern.

Fig. 6b is the same pattern for the case where the incident angle is changed to be equal to the angular radius of M2, i.e. so that the beam is focused onto the edge of M2. The plot shows how clipping by M2 then effectively cuts the beam in half. In the present model where the surround is fully absorbing, only the part of the beam shown is propagated onwards. The case shown corresponds to approximately 50% clipping, i.e. it is an angle close to the 50% point of the instrument PSF response.

Figures 7 a & b show the beam patterns at the instrument pupil stop, for the same cases as in fig.6 a & b, and in this model clipping by the intervening components between M2 and the stop is assumed to be absent. In fig. 7a the beam has similar form to the centrally-obscured beam of fig.5, but with some blurring of the edges due limited of spatial resolution in the numerical analysis. Fig.7b shows the same pattern for the off-axis case, and here it can be seen that the clipping of fig.6b results in a spreading of the beam pattern in the direction perpendicular to the clipping edge (the Y-direction in both plots), as is as expected from spatial filtering considerations.

At the stop the beam is again clipped, by the finite size of the pupil stop aperture, and the beam patterns after clipping (i.e. in the plane just after the stop) are shown in figures 8 a & b. The spreading of the beam shape means that the clipping of the beam by the instrument pupil stop is more severe in case (b) than in (a). Thus there is a knock-on effect whereby beam

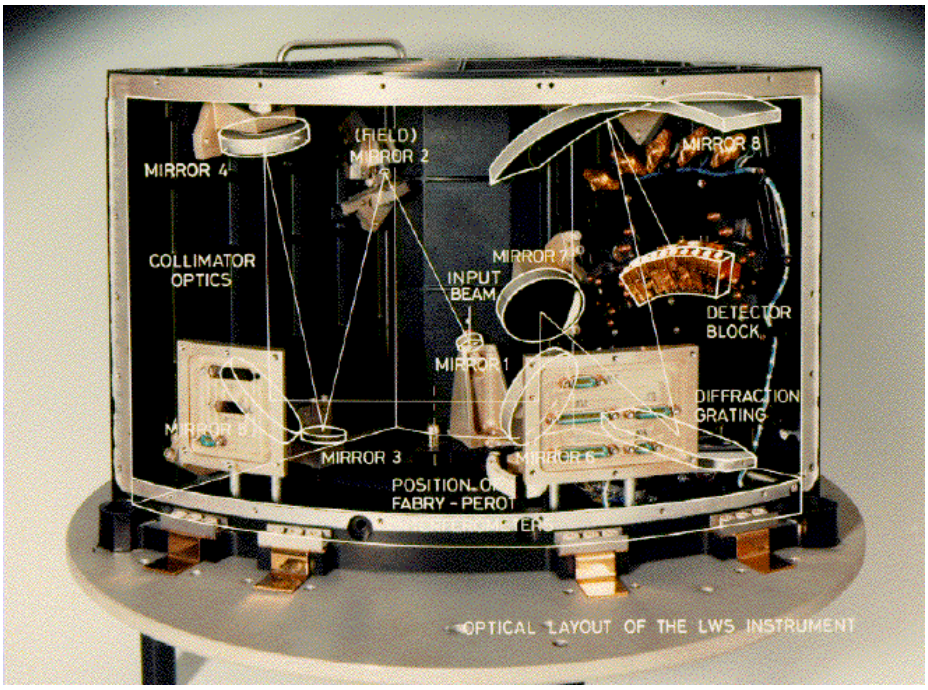

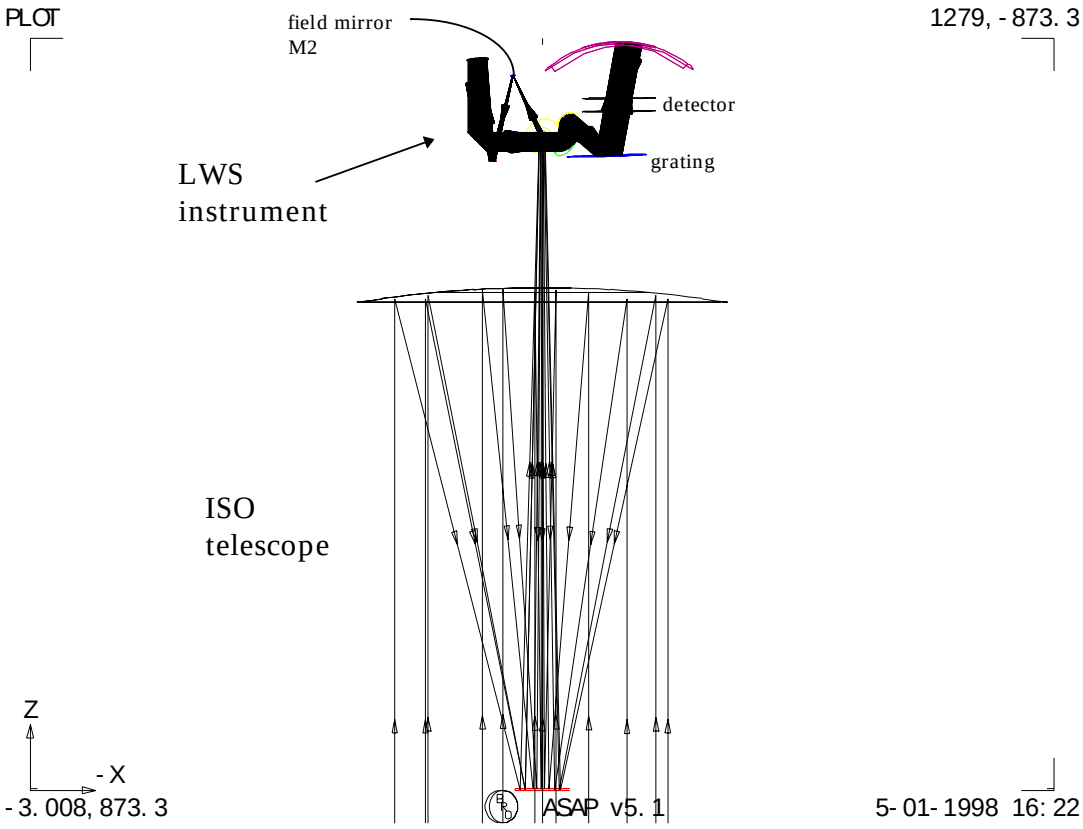

Fig.4 (a) photo of LWS showing optical path and (b) ray-trace model of ISO + LWS, for single collimated input beam.

clipping at one component (M2) leads to increased clipping at another (the pupil stop), so that the net transmission is less than the 50 % expected. This would correspond to a reduction in the FWHM of the PSF, i.e. a narrowing, as observed experimentally.

To test this, the full PSF response is simulated by re-running the above beam propagation over a range of off-axis angles. For each angle the energy which passes the pupil-stop, i.e. that contained in the patterns of fig.8, is recorded as that detected (i.e. we assume the subsequent has 100% detection efficiency). The resulting PSF is plotted in fig.9, along with that obtained when it is assumed that clipping by M2 alone determines the PSF (i.e. assuming that the energy collected by M2 is all detected). The figure shows that the reduction in FWHM of the PSF is by approximately 5% in this model.

The narrowing seen in the actual experiment is 13%, and the remaining discrepancy between model & experiment is attributed to the fact that the model includes clipping by only 2 components, whereas it is probable that clipping by other components is also playing a part. A full quantitative model of the PSF (needed for calibration purposes) will therefore require a careful re-assessment of all component sizes in the instrument & inclusion of their clippings in the model.

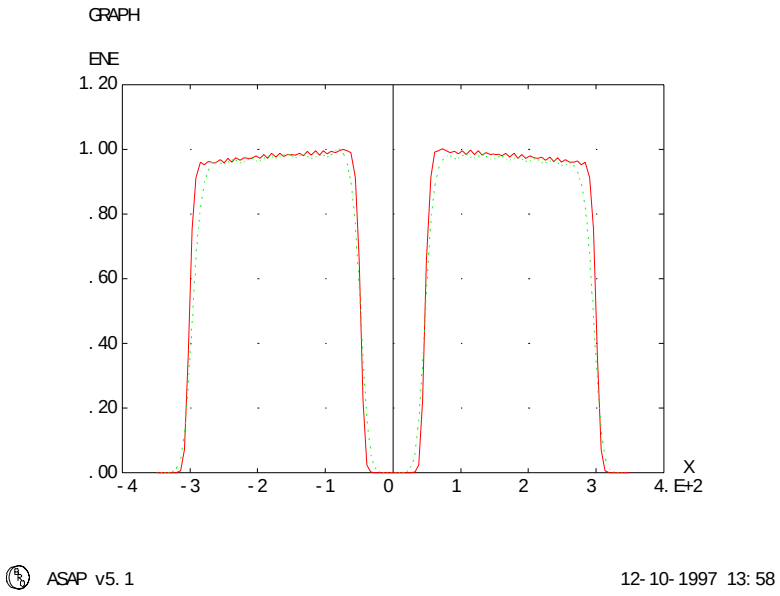

Fig.5. Cross-section of beam pattern at Telescope primary mirror.

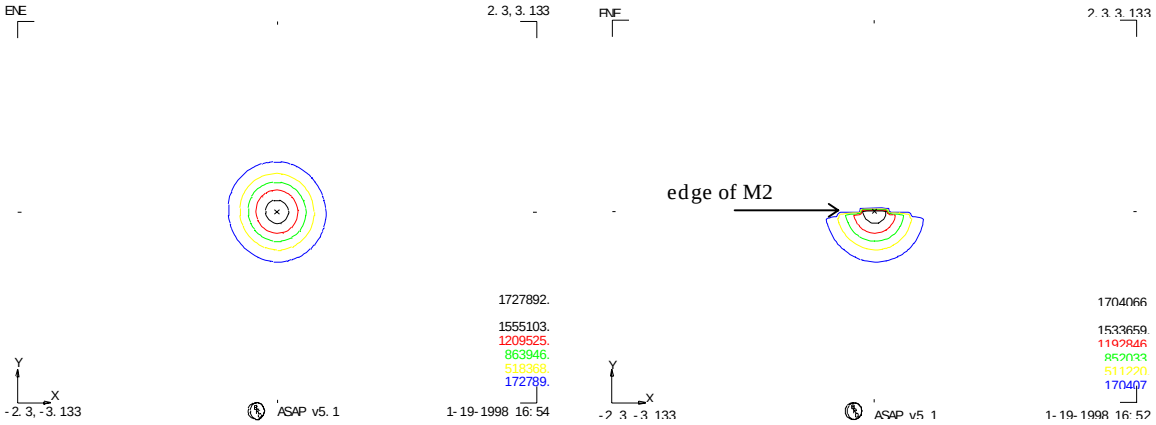

Fig.6. Beam pattern at M2 (a)(left) for on-axis beam (b)(right) for off-axis beam.

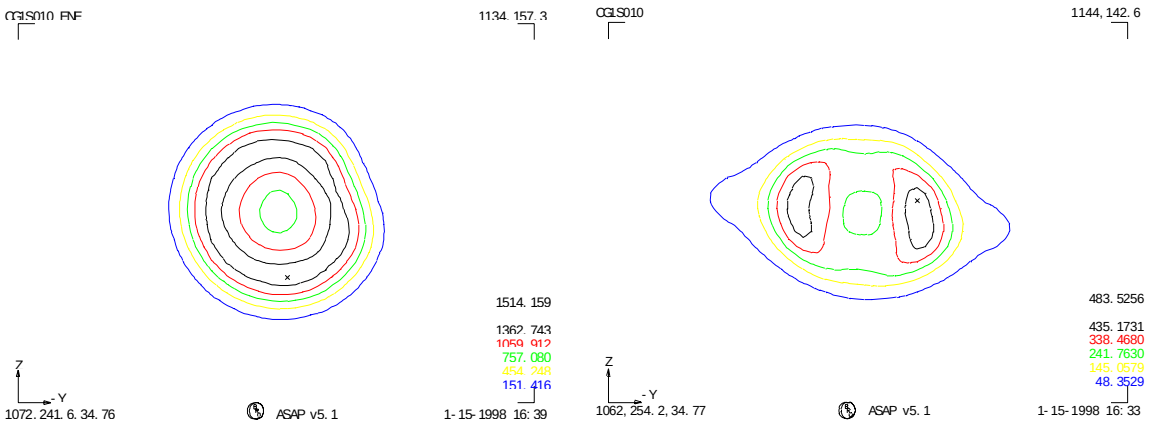

Fig.7 Beam pattern at instrument pupil stop, before clipping (a) (left) on-axis (b) (right) off-axis.

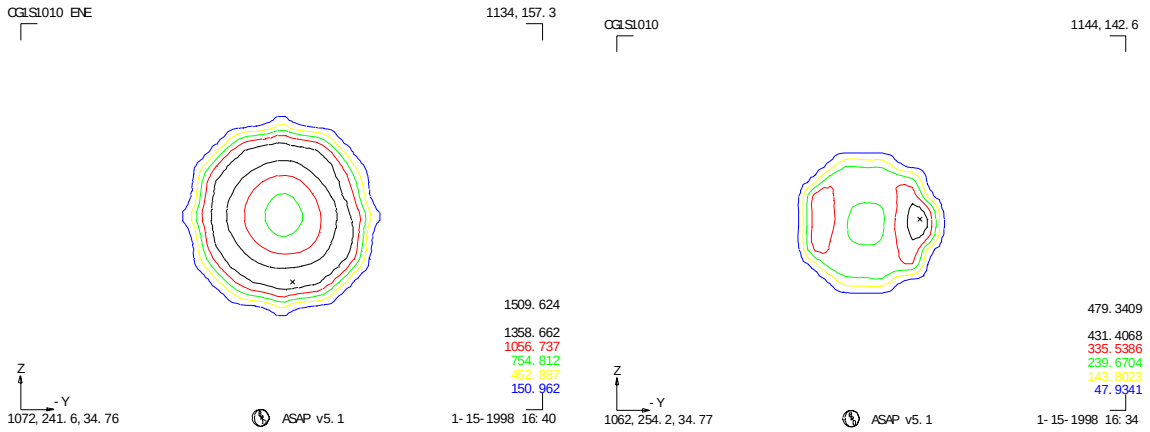

Fig.8 Beam pattern at pupil stop, after clipping (a) (left) on-axis (b)(right) off-axis. The non-circular beam edge is due to pixellation effects.

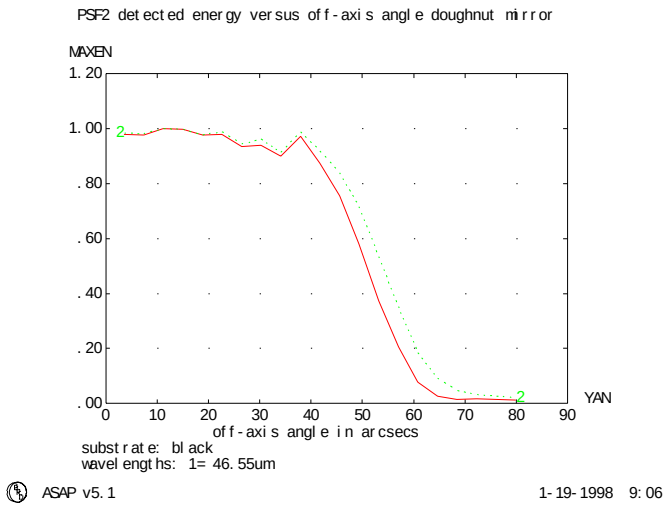

Fig.9. Predicted PSF curves at 46µm wavelength, normalised. Dotted line: no stop clipping, solid line: with stop clipping.

6. SPIRE INSTRUMENT ON FAR-INFRA-RED SPACE TELESCOPE (FIRST).

This instrument, shown in figure 10, is currently in the design phase. It is an imaging photometer system utilising 3 arrays of detectors to obtain filter-defined wavelength bands centred on 250, 350 & 500 μm.

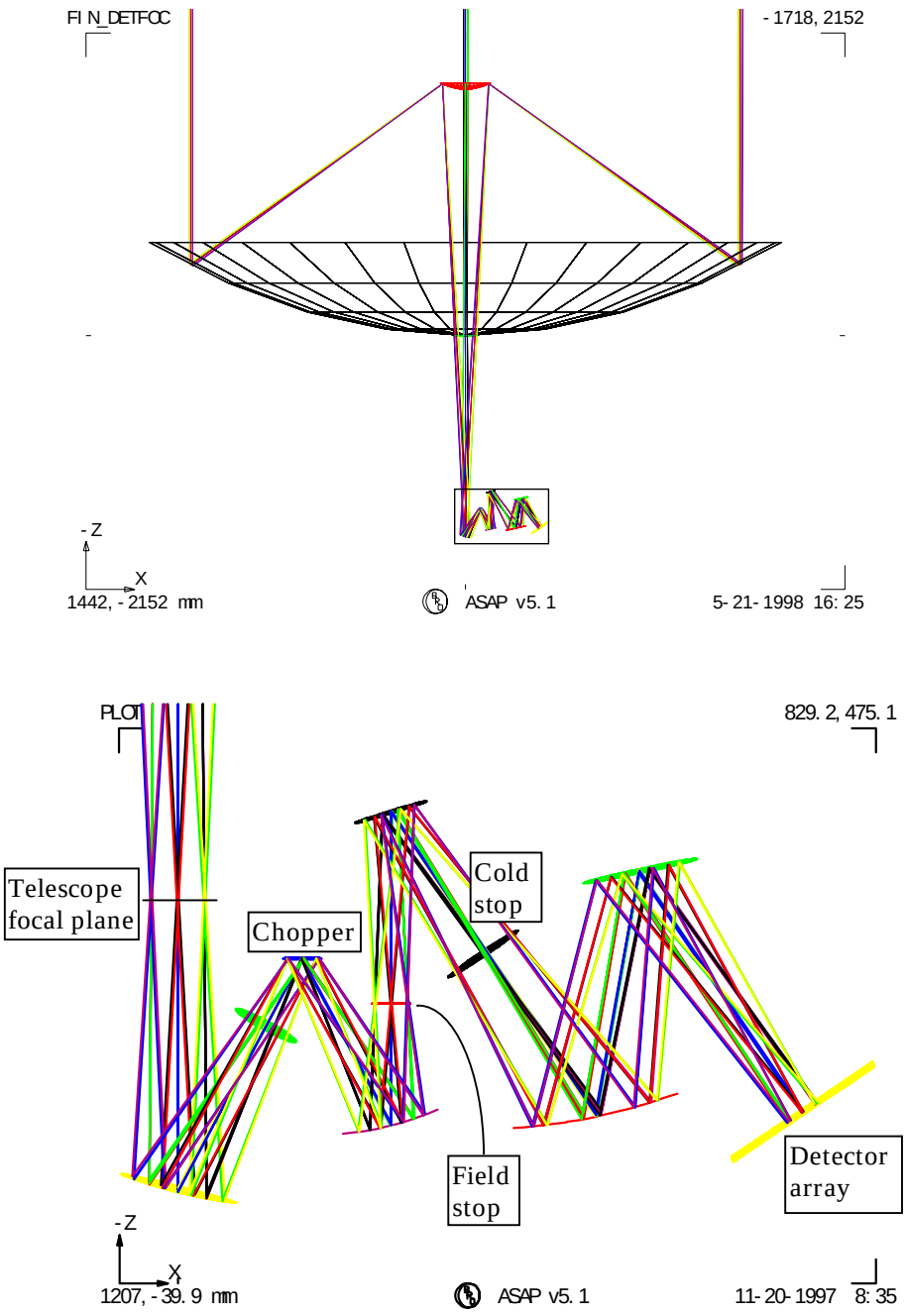

Figure 10. FIRST-SPIRE instrument. Upper plot shows relation to FIRST telescope, lower plot is expanded view to show photometer design.

Here the beam propagation analysis is needed to determine the component oversizes required in order to avoid beam-clipping problems such as those described above. The analysis proceeds in the reverse direction beginning at the detector. The type of detector (and therefore the beam shape) is not yet finalised for this instrument, but one possible choice is a

'bare' bolometer (low spatial coherence), for which the beam pattern corresponds to a point source at the centre of the detector. After clipping by the cold stop (assuming intervening optics are oversized with respect to this) the beam has a top hat profile as shown in figure 11.a. Here the pattern is calculated at both the longest SPIRE wavelength (0.5mm) and at a shorter wavelength (25μm) to show the shape of the geometric beam. The more sloping edge in the long wavelength plot is due to the spatial resolution limitation outlined in section 4.

This beam is propagated outwards through the system, and its profile is calculated at each component to determine oversizes required for stray light control. Of particular importance is the pattern in the telescope, since this is relatively hot. For example, the telescope secondary mirror is also at a pupil plane, and using imaging theory it is expected that at this component the edge of the beam pattern will be blurred due to diffraction, to a blur diameter of $b = 2.44\lambda F$, where F is the f-number of the ray bundle which connects the pupils at the instrument cold stop and the telescope. This is determined by the size of the intervening field stop, and at the telescope M2 it has a value of F= 60 , giving b=70 mm.

Figure 11.b shows the beam pattern at M2. Here the beam diameter is 270mm, and the expected diffractive blurring of the long wavelength pattern is clearly evident.

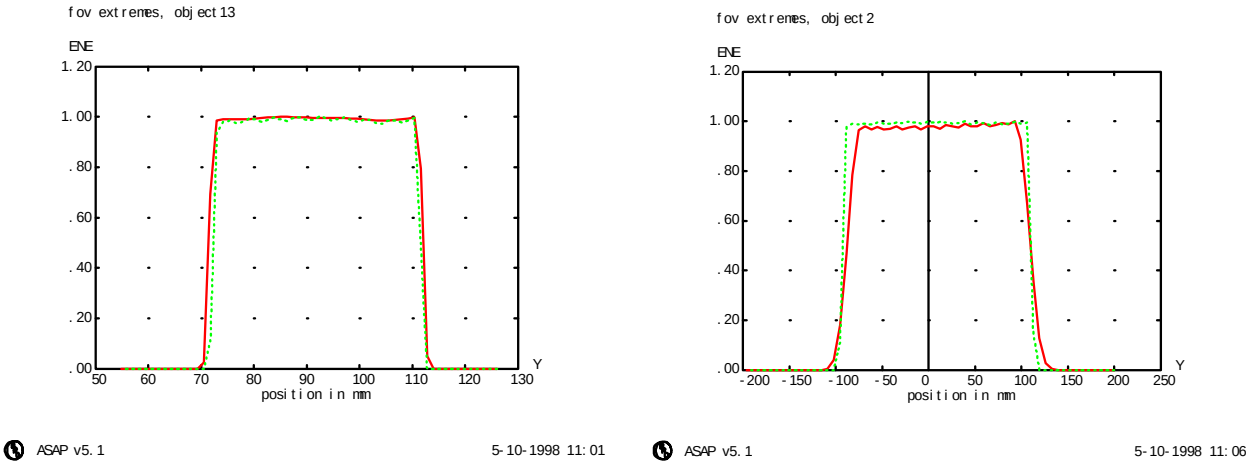

Figure 11 Beam profiles (a) (left) at cold stop, (b) (right) at telescope pupil M2. Horizontal scale is in mm. Dotted line is geometric beam, and solid line is beam at λ=0.5mm.

This diffractive spreading of the beam is problematic, because it means that the detector will 'see' the surround outside the edges of M2 , and this is relatively very hot and may have high emissivity. The solution would be to undersize the instrument pupil with respect to that of the telescope (so that more of the instrument's beam pattern falls within M2), and this is equivalent to the Lyot stop in a forwards-propagation model.

However, this undersize leads directly to a loss of system throughput, since then not all of the telescope's collecting power is used. Furthermore the throughput loss is at all wavelengths, whereas the stray light problem is worst at the longest wavelength (e.g. 0.5mm here). In systems with such wide wavelength coverage it is therefore not acceptable to design for avoidance of beam clipping at the longest wavelength, as this gives poor overall throughput. Rather, there is a trade-off between loss of performance at the long wavelength end, and overall throughput. As a consequence of this the of multiple beam-clipping phenomena becomes an important aspect of design.

7. CONCLUSION.

We have considered the importance of MBC effects in IR instruments in region ≥ 50μm, for FOV response and stray light control. A beam propagation analysis which can efficiently include such effects has been described and its current limitations explained. Examples were then given of two analyses cases for real instruments, one part of a post-launch diagnosis and the other part of a design study. These examples show the practical importance of the MBC effect, and it is expected that this type of analysis will be needed in other forthcoming IR instruments. The software model described here

will be developed to allow cases intermediate between the current far field/near-field cases, and to improve the spatial resolution with which edge-clipping is described.

8. ACKNOWLEDGEMENTS.

This work was supported by the ISO-LWS and FIRST-SPIRE projects, both funded by the UK Particle Physics & Astronomy Research Council (PPARC).

9. REFERENCES.

1. E. R. Freniere R.D.Stern & J.W.Howard, "SOAR: a program for the rapid calculation of stray light on the IBM PC." SPIE Vol.1331 *Sray radiation in optical systems* pp.107-117. 1990.

2. D H Martin & J W Bowen. "Long-wave optics" IEEE Trans. on microwave theory & techniques, Vol.41, No.10. Oct.1993.

3. A. W. Greynolds. "Propagation of generally astigmatic gaussian beams along skew ray paths" SPIE Vol.560 *Diffraction phenomena in optical engineering applications* pp.33-50. 1985.

4. Advanced Systems Analysis Program (ASAP©). Version 4.0 (1995). Publ. Breault Research Org. Inc. 6400 East Grant Road, Tucson, AZ, USA.

5. P Einziger et al."Gabor representation and aperture theory." Journal of the optical society of america (JOSA), Vol.A3, No.4, pp.508-522. 1986.

6. J. W. Goodman *Introduction to Fourier Optics* McGraw-Hill, New York 1968.

7. M. Satter. "Computer modelling of slit diffraction" SPIE Vol.1753 p.105 . 1992.

8. A. W. Greynolds. "Method for calculating diffraction effects in opto-mechanical systems of arbitrary geometry" Proc. SPIE. Vol.257,pp.64-77. 1980.

9. R J Martin & D H Martin. "Quasi-optical antennas for radiometric remote-sensing" IEE. Electronics & Communication Engineering Journal. Feb. 1996.

10. B. Swinyard. "In-orbit performance of the ISO long wavelength spectrometer" SPIE Vol.3354. 1998.